ACS OMEGA

http://pubs.acs.org/journal/acsodf

Article

Antibacterial Porous Electrospun Fibers as Skin Scaffolds for Wound Healing Applications

Georg-Marten Lanno, Celia Ramos, Liis Preem, Marta Putriņš, Ivo Laidmäe, Tanel Tenson, and Karin Kogermann*

Cite This: *ACS Omega* 2020, 5, 30011−30022

Read Online

ACCESS | Metrics & More | Article Recommendations | Supporting Information

ABSTRACT: Electrospun fiber scaffolds have a huge potential for the successful treatment of infected wounds based on their unique properties. Although several studies report novel drug-loaded electrospun fiber-based biomaterials, many of these do not provide information on their interactions with eukaryotic and bacterial cells. The main aim of this study was to develop antibacterial drug-loaded porous biocompatible polycaprolactone (PCL) fiber scaffolds mimicking the native extracellular matrix for wound healing purposes. Mechanical property evaluation and different biorelevant tests were conducted in order to understand the structure−activity relationships and reveal how the surface porosity of fibers and the fiber diameter affect the scaffold interactions with the living bacterial and eukaryotic fibroblast cells. Cell migration and proliferation assays and antibiofilm assays enabled us to enlighten the biocompatibility and safety of fiber scaffolds and their suitability to be used as scaffolds for the treatment of infected wounds. Here, we report that porous PCL microfiber scaffolds obtained using electrospinning at high relative humidity served as the best surfaces for fibroblast attachment and growth compared to the nonporous microfiber or nonporous nanofiber PCL scaffolds. Porous chloramphenicol-loaded microfiber scaffolds were more elastic compared to nonporous scaffolds and had the highest antibiofilm activity. The results indicate that in addition to the fiber diameter and fiber scaffold porosity, the single-fiber surface porosity and its effect on drug release, mechanical properties, cell viability, and antibiofilm activity need to be understood when developing antibacterial biocompatible scaffolds for wound healing applications. We show that pores on single fibers within an electrospun scaffold, in addition to nano- and microscale diameter of the fibers, change the living cell−fiber interactions affecting the antibiofilm efficacy and biocompatibility of the scaffolds for the local treatment of wounds.

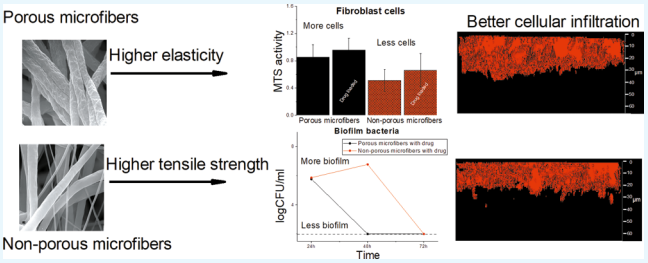

1. INTRODUCTION

Treatment of wounds is a major concern worldwide as the wound care costs are increasing every year. During the last few years, the development of electrospun skin scaffolds and fibrous wound dressings and matrices has been introduced as alternatives to traditional wound care products to address the problem.[1]

Electrospinning is a straightforward method for producing ultrafine fibers with nano- to micrometer range diameters and with controlled surface morphology. The fibers have unique characteristics, for instance, large specific surface areas and long length scales.[2] Furthermore, the fibers can be used as novel drug delivery systems (DDSs) which enable the modification and control of the drug release.[3] Over the past few years, several poorly water-soluble active pharmaceutical ingredients have been incorporated into nanofibers in order to obtain a modified drug release. Drug release from nanofibers is mostly explained to be based on diffusion, hence the porosity of the single fibers as well as the porosity and stiffness of the entire fiber scaffold can modify this effect.[4] However, it has also been shown that in case when 100% release from fibers is not achieved, desorption of embedded drug from nanopores in the fibers or from the outer surface of the fibers in contact with the release medium is the main mechanism.[5] Differences in drug release may have different effects on the antibacterial/antibiofilm activity of the fiber scaffolds.[3,6,7]

Fibers produced by electrospinning are known to have several advantages in wound healing, as widely reported in recent publications.[8,9] Among other advantages, nanofibers have an extracellular matrix type structure, a high specific surface area, and a porous structure which can absorb the wound exudate and enhance the oxygen permeability.[3] Functionalization of the fibers with antimicrobial drugs adds another dimension and enables the fight against wound

Received: September 9, 2020
Accepted: November 3, 2020
Published: November 12, 2020

https://dx.doi.org/10.1021/acsomega.0c04402
ACS Omega 2020, 5, 30011−30022

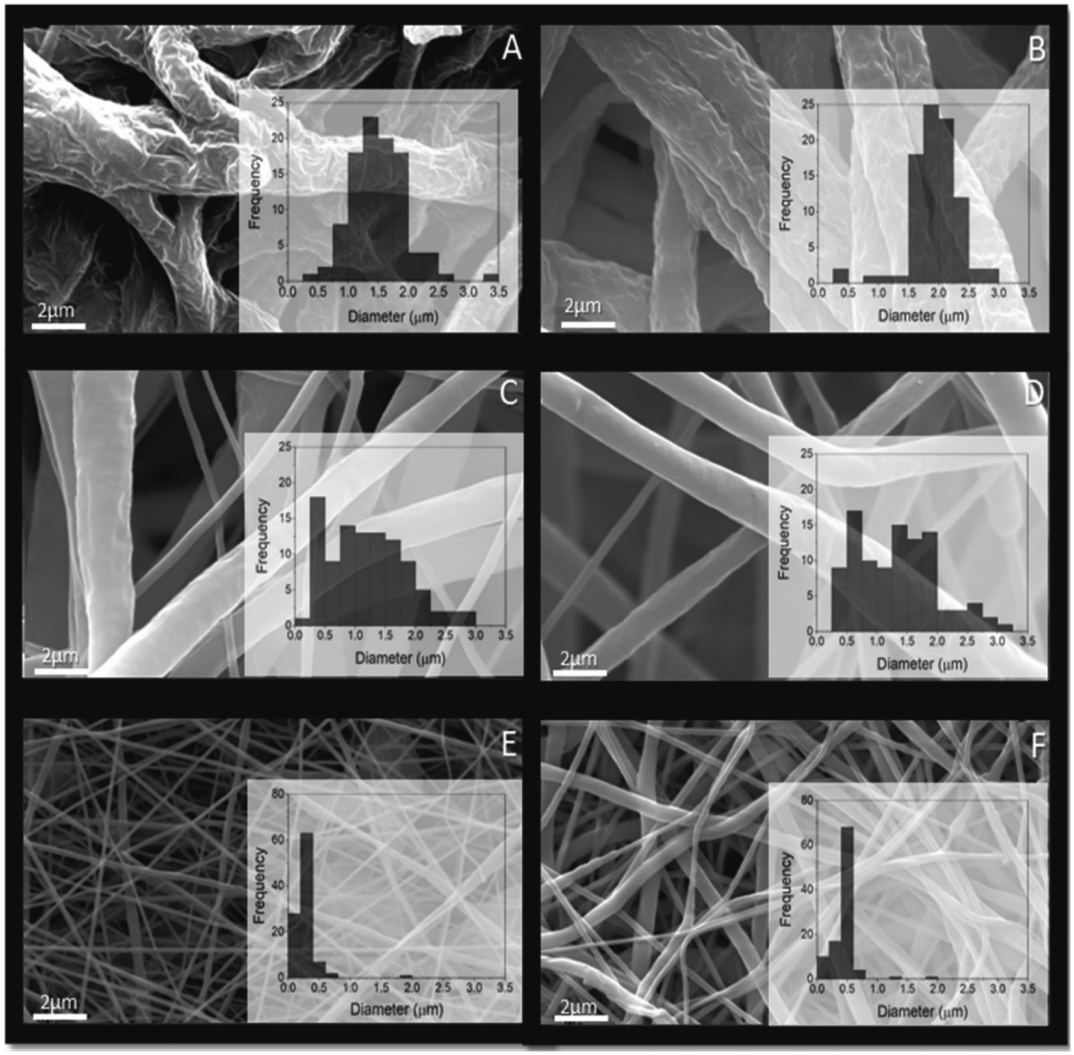

Figure 1. SEM micrographs of porous and nonporous electrospun PCL microfiber and nanofiber scaffolds without and with CAM (magnification 10,000×) with histogram insets. Porous microfibers, obtained using the THF/DMSO solvent system at high RH without (A) and with CAM (B). Nonporous microfibers, obtained using the THF/DMSO solvent system at low RH without (C) and with CAM (D). Nonporous nanofibers obtained using the AA/FA solvent system at low RH without (E) and with CAM (F). Key: AA—acetic acid; CAM—chloramphenicol; DMSO—dimethyl sulfoxide; FA—formic acid; PCL—polycaprolactone; RH—relative humidity; THF—tetrahydrofuran.

infections, which is one of the major causes for chronic wound and wound complication development.

Electrospinning allows producing fibers with different morphologies and structures (e.g., porosity, alignment) from chemically different polymeric materials and active substances (antimicrobial agents, growth factors, etc.). From the wound healing point of view, in addition to the selection of suitable scaffold materials, the fiber scaffolds need to have certain stiffness and porosity to ease the cell attachment, migration, and proliferation. It is known that cells attach to and interact with fibers differently than with flat substrates. Cells sense and respond to changes in structural stiffness by increasing the spreading on regions of higher stiffness.[10] Mechanical properties such as the strength and deformability of nanofiber scaffolds influence *in vitro* cell migration, proliferation, and differentiation, along with cell morphology.[11] A decreased fiber diameter has been shown to correlate with improved mechanical properties of the scaffolds.[12,13] Whereas the combination of both micro- and nanofibers enhances cell penetration and infiltration to the matrix as it creates greater pore interconnectivity and larger pore size.[14] It has been shown with several DDSs that the mechanical properties of materials may play a part in drug loading, drug−polymer interactions, release behavior, drug partitioning, and polymer degradation.[15]

It is desired that materials as well as mechanical properties of the developed fiber scaffolds are similar to those of the skin. However, it is not known what kind of electrospun matrix material and structure supports the wound healing the best and provides the best protection from bacteria. Several studies have investigated the effect of scaffold porosity on cell interaction,[16,17] but only few studies have addressed the effect of surface porosity of drug-loaded fibers on cell behavior and cell−fiber interactions.[18,19] Therefore, it is of interest to reveal whether pores on single fibers within the electrospun scaffold, in addition to nano- and microscale diameter of the fibers, change the living cell−fiber interactions. Interactions between the electrospun matrix with bacteria and eukaryotic cells determine the antimicrobial efficacy and safety of the antimicrobial scaffolds for the local treatment of the wound.

The aim of this study is to understand the structure−activity relationships and reveal how the fiber diameter and surface porosity of single fibers affect their interactions with the

https://dx.doi.org/10.1021/acsomega.0c04402
ACS Omega 2020, 5, 30011−30022

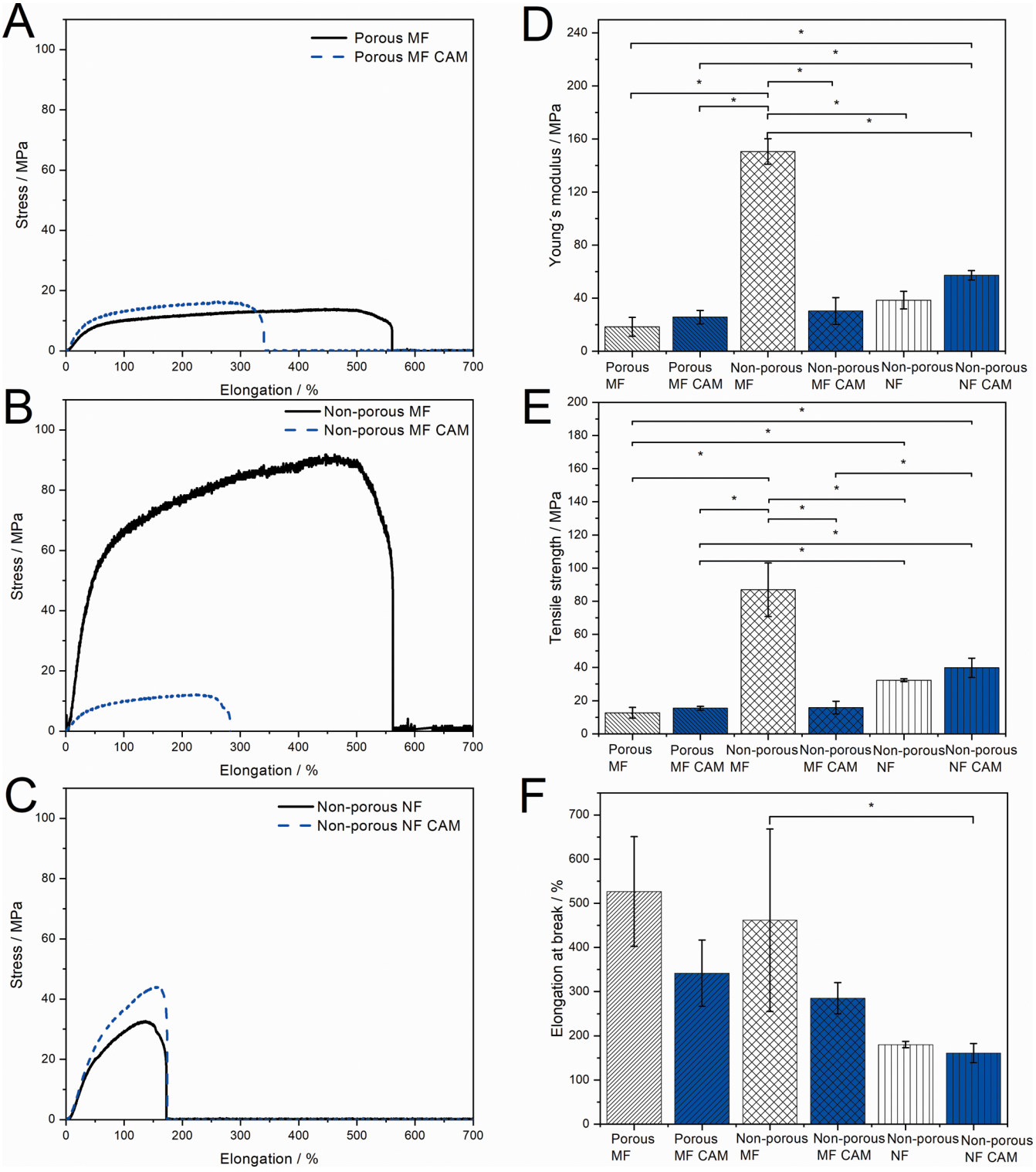

Figure 2. Mechanical properties of dry porous and nonporous electrospun PCL microfiber and nanofiber scaffolds without and with CAM. Representative stress−strain curves of the (A) porous MF, (B) nonporous MF, and (C) nonporous NF scaffold; (D) Young's modulus; (E) tensile strength at break; and (F) elongation at break. Data are presented as mean ± SD ($N = 3$). * Statistical significance, $p < 0.05$. MF = microfiber; NF = nanofiber.

bacterial and eukaryotic fibroblast cells. The mechanical properties of fiber scaffolds revealed the effect of fiber morphology and structure on the behavior of scaffolds. Cell attachment, proliferation assays, and antibiofilm assays enabled us to enlighten the biocompatibility and safety of the fiber scaffolds and their suitability to be used for the treatment of infected wounds.

2. RESULTS AND DISCUSSION

2.1. Morphology. Porous (pores on single fibers) and nonporous microfiber scaffolds were electrospun by recently

https://dx.doi.org/10.1021/acsomega.0c04402
ACS Omega 2020, 5, 30011−30022

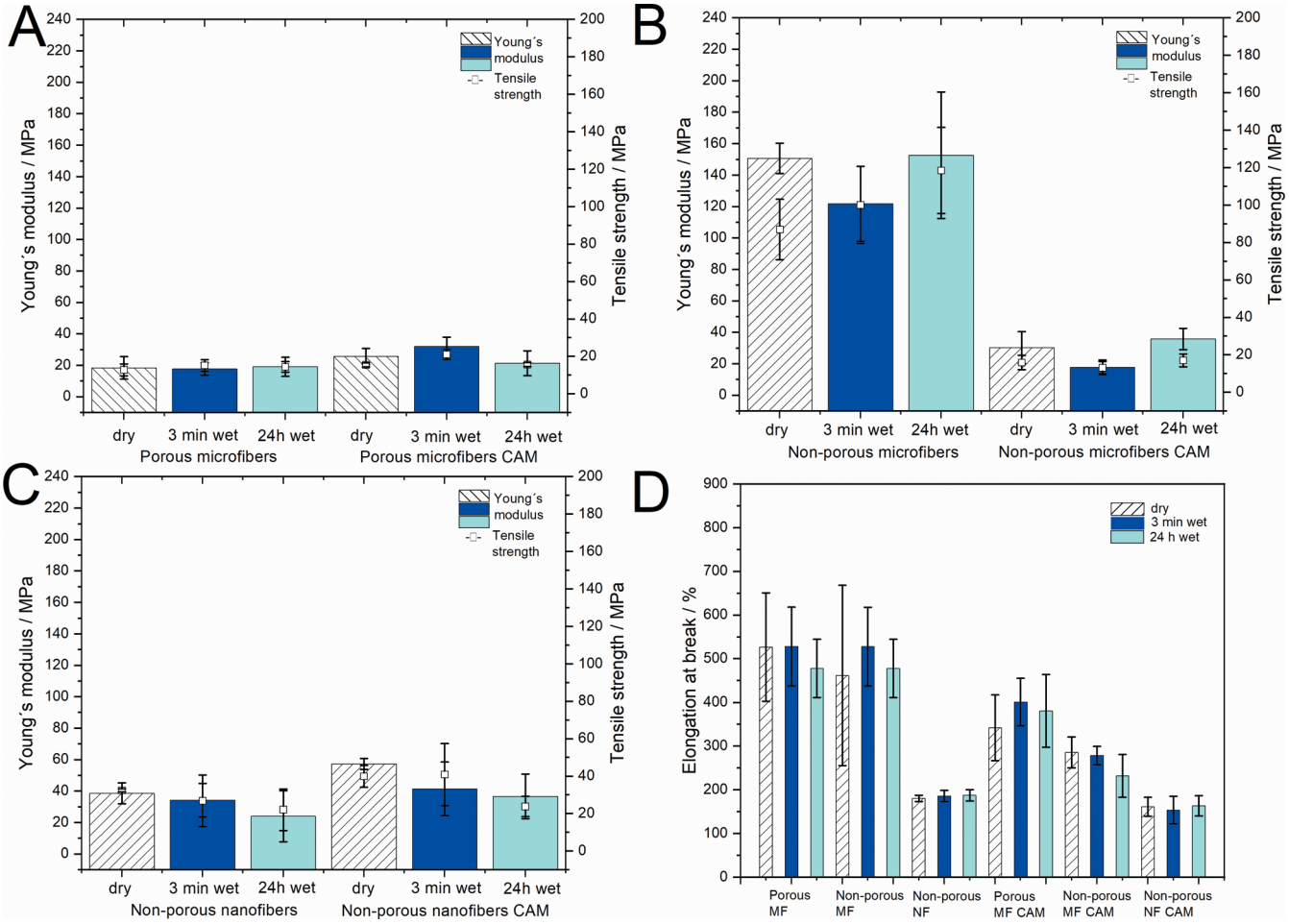

Figure 3. Mechanical properties (Young's modulus, tensile strength, and elongation at break) of dry and wet (3 min wet and 24 h wet) electrospun fiber scaffolds without and with CAM. (A) Porous microfibers without and with CAM; (B) nonporous microfibers without and with CAM; (C) nonporous nanofibers without and with CAM; and (D) elongation at break of all electrospun fibrous scaffolds. MF = microfiber; NF = nanofiber.

established approaches using polycaprolactone (PCL) 15 w/v % and tetrahydrofuran/dimethyl sulfoxide (THF/DMSO) (90:10 % v/v) under high relative humidity (RH) (65%) and low RH (19%) conditions (Figure 1).[20] The fiber diameters of porous fiber scaffolds ranged from 1.22 ± 0.21 (pristine) to 1.97 ± 0.30 μm (chloramphenicol [CAM]-loaded). The surface pore diameter was found to be 0.28 ± 0.08 for pristine porous microfibers and 0.22 ± 0.08 μm for CAM-loaded porous microfibers (Figure S1).

Nonporous nanofibers, obtained using the acetic acid (AA)/formic acid (FA) solvent system, had a smooth surface without any surface pores, and the fiber diameters ranged from 250 ± 110 (pristine) to 450 ± 110 nm (CAM-loaded). The fiber diameters of nonporous microfibers were 1.0 ± 0.48 (pristine) to 1.5 ± 0.65 μm (CAM-loaded). As expected, the largest pores between the fibers were detected for microfiber scaffolds (13.24−21.87 μm) and the smallest pores for nanofiber scaffolds (2.88−3.65 μm). Full morphology and solid-state characterization of these fiber scaffolds have been reported previously.[20]

2.2. Mechanical Properties. The fiber scaffolds consisting of porous and nonporous microfibers and nonporous nanofibers (pristine and CAM-loaded fiber scaffolds) showed different mechanical properties (Figure 2).

Nonporous microfiber scaffolds stretched the most before breaking (Figure 2B). Nanofiber scaffolds were more stiff and plastic compared to porous microfiber scaffolds (Figure 2A,C). The tensile strength and Young's modulus were the highest with nonporous microfiber scaffolds which were also found to be statistically relevant. Nonporous microfiber scaffolds had significantly higher tensile strength compared to the porous microfiber ones and increased Young's modulus values, indicating that the scaffolds behave differently in plastic deformation (Figure 2D,E). The elongation at break was found to be higher with porous microfiber scaffolds compared to that with nonporous nanofiber and microfiber scaffolds (Figure 2F). There was a trend showing a higher Young's modulus and tensile strength with nonporous nanofibers compared to porous microfibers. This correlates with the literature reporting that fibers with a smaller diameter have a higher tensile strength.[21,22] In general, drug-loaded fibers showed slightly increased tensile strength and Young's modulus except for nonporous microfibers but decreased elongation at break compared to those of pristine PCL scaffolds (Figure 2D−F). However, the latter was not statistically relevant for each composition. There exists a correlation between the macrostructural and microstructural porosities of fibers, which can be tracked by the free volume changes through the *ortho*-positronium (*o*-P) atom lifetime values.[23,24] The size of the free volume of pores (e.g., holes) determines the mechanical properties of the fibers and also the drug release from the

https://dx.doi.org/10.1021/acsomega.0c04402
ACS Omega 2020, 5, 30011−30022

samples.[25,26] The decreased free volume is known to increase the tensile strength of fibers.[27]

The mechanical properties of fiber scaffolds are very important for wound healing and tissue regeneration applications. In our study, the tensile strength was the highest for nonporous microfiber scaffolds compared to those of porous microfiber and nonporous nanofiber scaffolds (Figure 2E). In addition, the surface porosity on single fibers significantly increased the elasticity of the microfiber scaffolds shown in higher elongation at break values (Figure 2F). Previously, it has been stated that the tensile strength of PCL fibers increase significantly when the diameter of the fibers is reduced below 500 nm, however not in our case.[28] PCL fibers with larger diameters are known to increase the elongation at break, which was also confirmed in the present study (Figure 2F).[21] The scaffolds have to be strong enough to keep their structure when applied on the wounds and easily removable without damaging the newly formed tissue. For tissue scaffolds, the stiffness dictates the cell−fiber scaffold interactions.[29] Focal adhesions allow cells to push or pull themselves along the matrix, so the matrix should have sufficient stiffness to resist deformations by cell tractions; however, it is more complex with electrospun scaffolds where the cells can pull themselves in any direction.[30] While mimicking the skin, their mechanical properties can differ depending on their origin, but the tensile strength for the native skin is approximately 20 MPa[31] and Young's modulus range from 0.008 MPa[32] up to 70 MPa.[31] Elongation at break values for the skin range between 35 and 115%.[33]

It is believed that in addition to the fiber and fiber scaffold structure, the effect of solvents on the PCL structure (e.g., polymer crystallinity) needs to be taken into account, and this may change the mechanical behavior of the material.[34] We confirmed that the electrospinning solution composition and the diameter of the fibers together with the scaffold structure all affect the mechanical properties of PCL fiber scaffolds. Previously, several publications have characterized PCL electrospun fibers and fiber scaffold mechanical properties, and the values indeed vary significantly depending on the solvent system, fiber diameter, and scaffold structure and thickness.[35] Arinstein and Zussman have suggested that the relaxation process generated by evaporation of solvent within electrospun fibers can significantly affect the mechanical properties of polymeric nanofibers.[36] Electrospinning of PCL from AA is known to form brittle nanofibers that are less elastic.[37] Hence, the less elastic behavior of nanofiber scaffolds in addition to the fiber diameter may be related to the solvents (AA/FA) used for electrospinning.

Drug encapsulation can either increase or decrease the mechanical properties of electrospun PCL fibers.[22,38] It has been shown that incorporation of the antibacterial drug linezolid into PCL scaffolds improved their mechanical properties.[39] It is known that drug−polymer interactions affect the mechanical properties of electrospun polyester fibers,[15] and as the solid-state analyses in our previous study have revealed, different solvents may have affected the CAM−PCL interactions at the molecular level differently.[20] This may lead to different mechanical behavior of scaffolds. Addition of CAM to the scaffolds only slightly increased the tensile strength of porous microfiber and nonporous nanofiber scaffolds. However, the tensile strength and Young's modulus of nonporous microfiber scaffolds and the elasticity of all the samples were decreased (Figure 2).

In order to understand the mechanical properties of PCL scaffolds under wet conditions (e.g., mimicking wounds), the samples were introduced into the buffer solution for 3 min and 24 h (Figure 3).

After 3 min and 24 h in buffer, there were no significant changes observed in the mechanical properties of wet pristine PCL scaffolds compared to their respective dry scaffolds (Figure 3A−C). The elongation at break remained mostly unchanged for all samples (Figure 3D). Interestingly, no significant differences in mechanical properties (tensile strength and Young's modulus) were observed with CAM-loaded scaffolds after wetting (Figure 3C). The tensile strength of nonporous CAM-loaded nanofibers decreased under wet conditions from 39.86 (dry) to 23.78 MPa (24 h wet) most likely as a result of drug release; however, it was not found to be statistically relevant. Similarly, porous microfibers with CAM show similar trends in decreased tensile strength and Young's modulus values (Figure 3A).

2.3. Wettability, Swelling, and Early *In Vitro* Degradation Behavior. It is stated that higher buffer penetration increases the degradation of the matrix as well as the amount of drug released.[6,40] The nonporous pristine nano- and microfiber scaffolds showed a higher swelling index compared to those of porous microfiber scaffolds (Figure 4A). The highest swelling index was observed for nonporous microfibers, but this was not statistically significant. There were no relevant differences in the weight loss of scaffolds as the weight loss for all scaffolds was very low (Figure 4B). All CAM-loaded samples showed a higher swelling index and weight loss compared to those of pristine scaffolds (Figure 4A,B).

With electrospun fiber scaffolds, it has been previously shown that the smaller diameter (nanoscale) fibers increase the surface roughness and the fraction of the contact area of the droplet with the air trapped between fibers.[41] All pristine PCL scaffolds showed no statistical difference in contact angle values at the start of the experiment and after 30 s (Figure 4C); however, all CAM-loaded samples showed decreased contact angle values after 30 s in contact with the buffer. As expected, CAM-containing scaffolds showed more hydrophilic surfaces, as the drug started to dissolve and made it easier for the buffer to penetrate into the scaffold structure. Surface porosity of microfiber scaffolds most probably affected the surface roughness of the fiber samples, but the effect was not observed as a significant difference in contact angle values. It is known that the surface roughness increases together with the apparent contact angle of hydrophobic materials, while for hydrophilic materials the contact angle decreases.[42] Therefore, the wetting properties of more hydrophilic surfaces should be improved by increasing the surface roughness.

Fiber morphology and diameter may enormously affect the behavior of electrospun fiber scaffolds under biorelevant conditions, and consequently, their interactions with living cells, specifically if these scaffolds are functionalized with antimicrobial agents. PCL fibers are hydrophobic; however, the addition of CAM made the scaffolds more hydrophilic and induced the drug release, which has been shown previously.[3,43,44] Significant swelling occurred, and in addition to the increased swelling index, we also observed increased fiber diameters and changed morphology (Figures 4A and S2). Increased fiber diameters were more evident for nonporous fiber scaffolds which supports the swelling index results (Figures 4A and S2). However, only small degradation of scaffolds was seen within a short contact (24 h) with the

https://dx.doi.org/10.1021/acsomega.0c04402
ACS Omega 2020, 5, 30011−30022

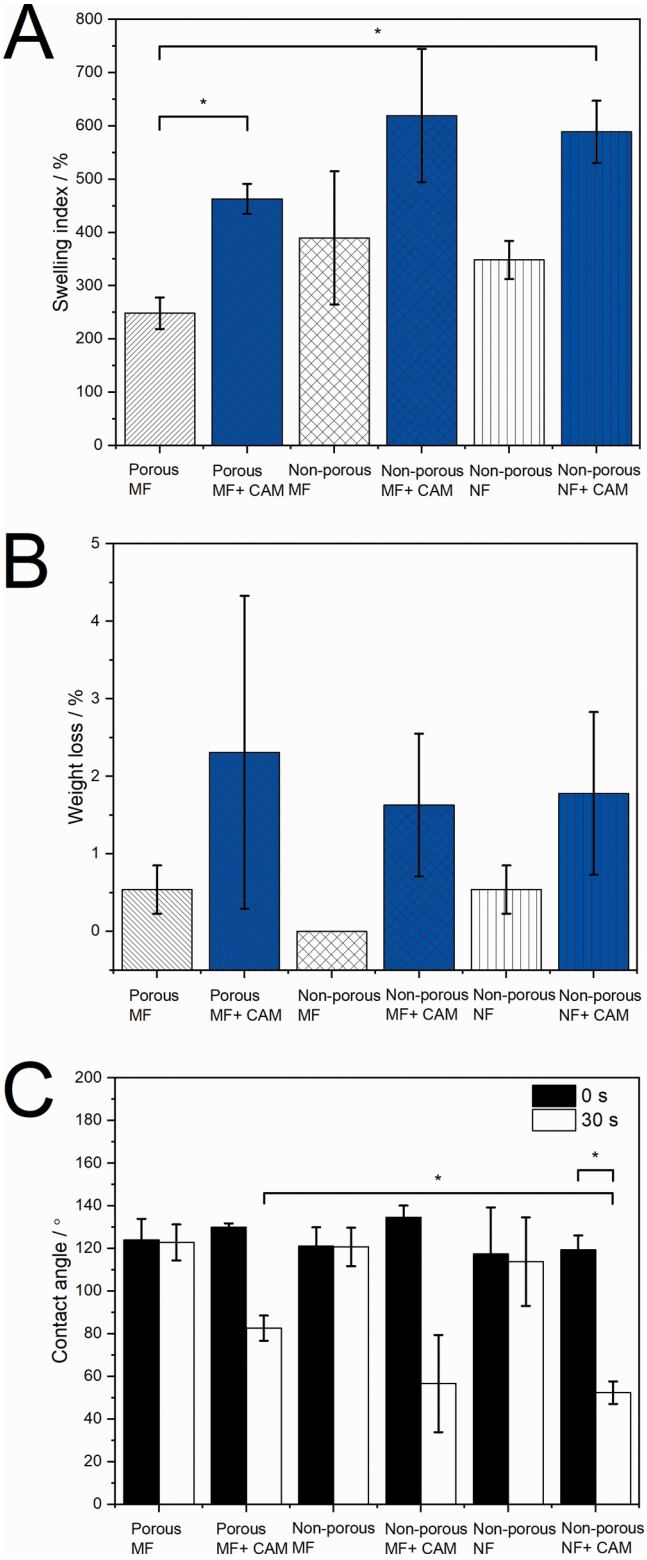

Figure 4. Swelling, weight loss, and wettability of electrospun fiber scaffolds when in contact with a buffer for different time periods. (A) Swelling index of all fiber scaffolds; (B) weight loss of all fiber scaffolds; and (C) contact angles of all fiber scaffolds at the start of the experiment and after 30 s. Data are presented as mean ± SD ($N = 3$). * Statistical significance, $p < 0.05$. MF = microfiber; NF = nanofiber.

biorelevant medium (Figures 4A,B and S2). In addition to wetting, drug release also takes place upon contact with the buffer. Our previous studies have revealed that the drug release from electrospun fiber scaffolds depends largely on the chemistry of the materials and structural properties of the mats. The CAM release from the present electrospun PCL fiber scaffolds showed differences. Fastest drug release was detected from nonporous nanofiber scaffolds, followed by porous microfiber and nonporous microfiber scaffolds. After 96 h, the nonporous nanofibers had released about 72.6% and porous microfibers 59.2% of CAM. In the case of nonporous microfibers, CAM was entrapped inside the fiber scaffold, and only about 20% of it was released within 96 h of testing.[20] The mechanical properties of PCL fiber scaffolds only slightly changed upon being in contact with the buffer (Figure 3). However, the contact angles of CAM-loaded scaffolds were significantly smaller compared to pristine scaffold values after 30 s in buffer, revealing better hydrophilicity of the samples (Figure 4).

2.4. Biological Relevance of Differently Designed Fiber Scaffolds. *2.4.1. Fibroblast Cell Attachment and Biocompatibility.* The fibroblast attachment and biocompatibility were evaluated using the MTS assay. The assay shows the metabolically active cells that react with the tetrazolium salt in MTS, which results in the production of soluble formazan dye. The highest absorbance was seen with porous microfiber scaffolds with CAM, which suggests that the cells had good attachment and proliferation properties and indicates that the nanoporous topology of the fiber scaffolds affects the behavior of fibroblast cells (Figure 5).

There was no statistically significant difference in MTS activity observed between porous and nonporous microfiber scaffolds with CAM. However, a clear trend was seen that the cells preferred to attach and proliferate on the porous microfiber scaffolds as these scaffolds showed higher MTS activity compared to that of nonporous microfibers, which was statistically significant ($p < 0.05$). The presence of CAM did not affect the behavior of cells on scaffolds during the testing time period (Figure 5A).

In order to understand the cell−scaffold interactions better, we tried to evaluate the fibroblast behavior and distribution on the scaffolds by confocal fluorescence microscopy (CFM). The 3D view-constructed micrographs from CFM can be seen in Figures 5C−E and S3. The red membrane dye used (FM4-64) shows the cellular placement and distribution throughout the scaffold. The highest number of cells together with the best infiltration properties was seen with the CAM-loaded porous scaffolds, where the cells were evenly distributed on the top level and infiltrated through the scaffold to the lowest depth (Figure 5C). This also correlates with the results of the MTS assay (Figure 5A). Figure 5D shows the cell infiltration for the nonporous microfiber scaffold. The cells were evenly distributed on the top layer of the sample and infiltrated similarly; however, the signal of the dye was lower than that observed for the porous scaffold one. The latter indicates the presence of a smaller number of cells on nonporous microfiber scaffolds compared to that of the porous microfiber scaffolds (Figure 5C). Furthermore, this correlates with the trends observed in the MTS assay (Figure 5A). With nonporous nanofiber scaffolds, the cells were evenly distributed only on the upper layer of the sample (Figure 5E).

Cell attachment and safety studies carried out with BHK-21 cells revealed that the structure of the PCL fiber scaffolds and single-fiber morphology (surface structure of a single fiber) have a huge effect on the cell behavior (Figure 5). It was seen that cells preferred to attach and penetrate more into the

https://dx.doi.org/10.1021/acsomega.0c04402
ACS Omega 2020, 5, 30011−30022

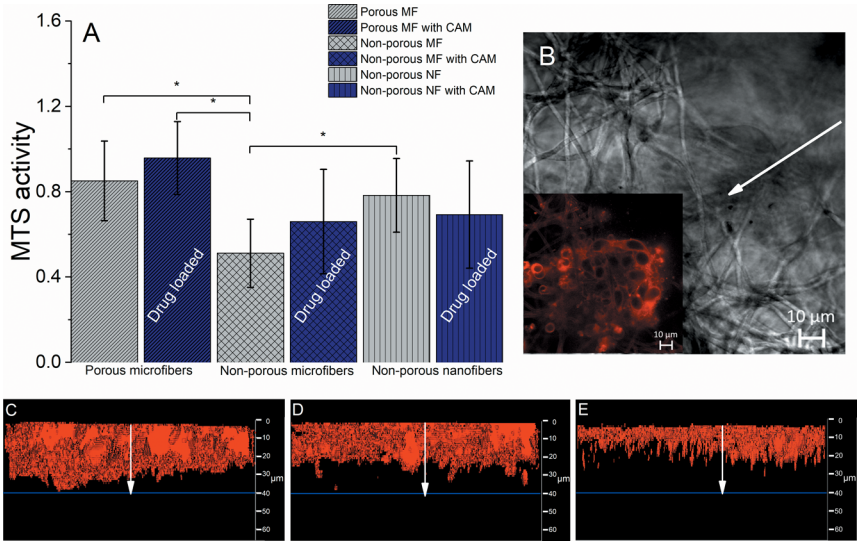

Figure 5. (A) MTS activity when fibroblast cells (BHK-21) were seeded onto porous and nonporous electrospun microfiber and nanofiber scaffolds without and with CAM (N = 3), * Statistical significance, $p < 0.05$. MF = microfiber; NF = nanofiber. Regarding exact formulations, reference is made to Figure 1. Cells were incubated for 48 h. (B) Confocal fluorescence microscopy (CFM) 2D micrograph of the porous microfiber scaffold in visible light with the inset picture (white arrow) of the same showing a fluorescent signal that comes from the FM 4-64 dyed fibroblast cells. CFM cross-section micrographs of fibroblast cells attached onto the electrospun (C) porous microfiber scaffold consisting of CAM; (D) pristine nonporous microfiber scaffold; and (E) pristine nonporous nanofiber scaffold. The white arrows in figures (C−E) indicate the fibroblast infiltration from 0 to 40 μm (blue line) in depth. Additional confocal images of the samples can be found in the Supporting Information (Figure S3) together with SEM images of BHK-21 cells on fibers (Figure S4).

microfibrous elastic scaffolds compared to that on nanofibrous less elastic scaffolds. Besides, the surface porosity of fibers and increased hydrophilicity (verified by lowered contact angle values and improved wettability), due to the drug release together with improved intrusion of aqueous medium into the scaffold structure, improved the attachment of cells on the scaffolds. The best cellular distribution and infiltration, compared to those of all the samples, were seen with porous microfiber scaffolds with CAM (Figure 5C), which also correlates with the results of the MTS assay (Figure 5A). The nonporous nanofiber scaffolds (Figure 5E) showed different cellular behavior as cells were distributed evenly only on the upper layer, and no cells were seen at lower depths. This phenomenon could be related to the fact that the pore size affects the cellular infiltration properties.[45]

It has been previously shown that cells are able to impregnate into the scaffold when its structure provokes it.[46] The pore size affects the cellular dimensions and the spreading capabilities.[45] One study about cellular growth dependency on the pore size of the matrix has suggested that fibroblasts tend to spread along the walls of the matrix in scaffolds with pore size above 20 μm, resulting in better infiltration properties, while pores with smaller sizes enhance the intercell communication and boost the extracellular matrix production. In the case of pores smaller than these cells, it has been stated that the cells migrate by the amoeboid movement deforming their cytoskeleton; however, the deformation is limited to about 10% of the nucleus size above which the degradation of the matrix comes into play.[47] Nanofibrous scaffolds have smaller pores than microfibrous scaffolds, so this limits the cellular penetration through the scaffolds which in turn leads to lower attachment and proliferation properties. We observed that the cells were more likely to attach and grow onto porous PCL microfiber scaffolds than on nonporous PCL microfiber scaffolds, which was also found to be statistically relevant ($p <$ 0.05). This states that the surface porosity of single fibers enhances the cellular attachment and proliferation properties in the scaffolds.

No significant differences were observed in the cell attachment between the drug-loaded and nonloaded porous microfiber scaffolds, revealing the biocompatibility and safety of CAM to be used in wound scaffolds within tested concentrations. It has been highlighted previously that PCL fibers and CAM at the concentration used are cytocompatible.[48,49]

Several studies have discussed that the porosity and mean pore size of electrospun fiber scaffolds affect the cell attachment and growth,[50] but to the authors' knowledge, only few studies have investigated the influence of single-fiber surface pores on cell behavior which was proven in this study. The effect of surface structure on the cell viability has been investigated before with PCL matrices supporting our findings.[34]

2.4.2. Bacterial Attachment and Biofilm Formation. No relevant differences were observed with planktonic bacteria comparing scaffolds with and without the drug (Figure 6A), however, not with the biofilm bacteria (Figure 6B). The results of *Escherichia coli* biofilm formation on different fiber scaffolds revealed that the electrospun fiber scaffolds without any CAM provide good surfaces for biofilm formation, and there are statistically significant differences in CFU values between the different fiber scaffolds after 48 h (Figure 6B).

Less biofilm was formed on porous and nonporous microfiber scaffolds than that on nonporous nanofiber scaffolds at 24 h time point, after which at 72 h time point, an increase in CFUs was seen on nonporous nanofiber scaffolds. With porous and nonporous microfiber scaffolds, the biofilm formation remained basically unchanged; only small differences were observed when nonporous microfiber and porous

https://dx.doi.org/10.1021/acsomega.0c04402
ACS Omega 2020, 5, 30011−30022

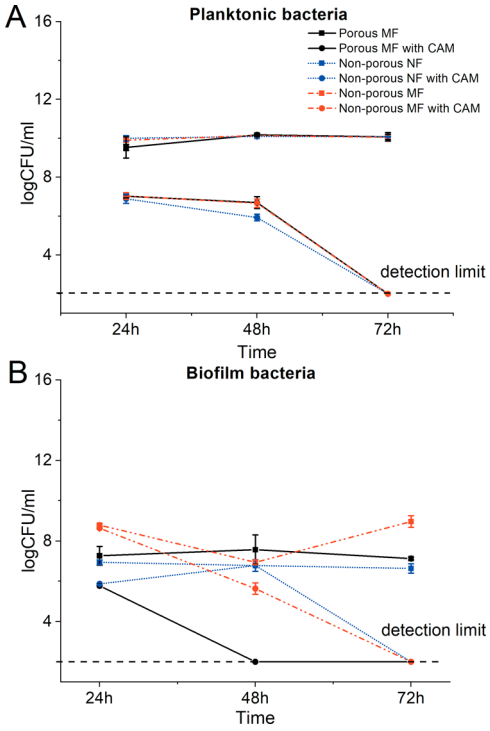

Figure 6. (A) Antibacterial activity of porous and non-porous electrospun PCL microfiber and nanofiber scaffolds without and with CAM on *E. coli* and (B) biofilm formation and antibiofilm activity. Regarding exact formulations, reference is made to Figure 1. Key: biofilm bacteria—biofilm bacteria washed off from the fiber scaffold; CAM—chloramphenicol; MF = microfiber; NF = nanofiber; planktonic bacteria—bacteria from the well where the fiber scaffold was removed. Detection limit refers to the CFU that can be counted by the plate method (200 CFU/mL).

microfiber scaffolds were compared, favoring the biofilm formation on porous microfiber scaffolds (Figure 6B).

The antibiofilm activity of CAM could be seen in all drug-loaded samples at all time points. The porous microfiber scaffolds with CAM showed the best antibiofilm activity compared to nonporous CAM-loaded nano- and microfiber scaffolds, which can be clearly seen at 48 h time point. After 24 h of incubation, the porous microfiber and nonporous microfiber scaffolds with CAM showed similar antibiofilm activity, whereas nonporous nanofiber scaffolds with CAM were not as efficient. After 72 h, all the drug-loaded samples had inhibited the bacterial growth.

Fiber diameter is known to affect the ability of bacteria to proliferate within the fibrous networks, depending on the cell size and shape; the highest proliferation occurs when the fiber diameter is close to that of the bacterial size.[51] However, it was recently reported that the biofilm formation on nanofibrous PCL scaffolds (electrospun from the chloroform/ethanol mixture) takes place and largely depends on the way bacteria attach onto the fiber.[52] The bacterial attachment is dependent on the fiber size (preferably, at a fiber diameter of 100 nm) and fiber coating. Organic substances of bacterial origin are a conditioning film (e.g., coating) for interactions between bacteria and nanofibers. The latter was found to play a remarkable role in facilitating the subsequent adhesion of bacterial cells to the PCL nanofibers (much smaller size compared to that of bacteria).[52] Similarly, in a recent study, a bacterial biofilm was formed on a scaffold comprising flat nanofibers (with an average fiber diameter of 390 nm).[53] In order to understand the bacterial attachment on the fiber surface and the relevance of different fiber structures for bacterial biofilm formation and potential antibiofilm activities of the drug-loaded fiber scaffolds, biofilm formation assays were conducted (Figure 6A,B). We also observed that biofilm formation was favored on nanofiber scaffolds compared to that on microfiber scaffolds. The surface topography largely affects the biofilm formation via different mechanisms, and surfaces with topographic features of dimensions in the submicrometric or nanometric range have been reported to inhibit attachment by reducing the contact area between bacterial cells and the surface.[54,55] Furthermore, nanoscale surface pores can create energetic situations unfavorable for bacterial attachment and induce repulsive surface−bacteria interaction forces that impair attachment and subsequent biofilm formation.[56,57] In our study, the surface properties (surface porosity) only slightly affected the biofilm formation, and in contrast to what was expected, more biofilm was detected on fibers with surface pores (Figure 6B).

With the drug-loaded fiber scaffolds, we have shown that the drug release rate and the amount of drug left within the sample[20] also affect the *E. coli* biofilm formation, and controversial results can be obtained if nanofibers release the drug faster compared to that of microfibers (Figure 6B). Fiber wettability, surface charge, and chemistry affect the ability of bacterial cells to attach and proliferate throughout the nanofiber scaffolds.[58] We have previously shown that non-porous nanofiber scaffolds exhibit faster drug release.[20] Therefore, less drug remained in those fibers, and *E. coli* biofilm formation was not as effectively hindered. Microfiber scaffolds had a lower drug release rate, and more drug was still within the fibers compared to nanofiber scaffolds providing better antibiofilm properties. Besides, antibacterial properties of CAM-loaded PCL fibers on planktonic bacteria were observed, which nicely correlated with the drug release profiles of the PCL fibers previously published for studied scaffolds.[20] Unfortunately, all tested electrospun fiber scaffolds acted as good surfaces for *Pseudomonas aeruginosa* biofilm formation, and no antibacterial or antibiofilm effect was detected with CAM-loaded PCL fiber scaffolds (Figure S5). These results were not surprising as *P. aeruginosa* is known to exhibit resistant behavior against CAM.[59,60]

3. CONCLUSIONS

Antibacterial CAM-loaded porous biocompatible PCL fiber scaffolds for infected wound-healing purposes were developed. PCL fiber scaffolds electrospun using different solvent systems show relevant differences in their morphology, structure, and elastic behavior, affecting their interactions with living cells (bacterial and eukaryotic cells). It is known that electrospinning allows the fabrication of differently designed structures; however, for the first time, the effect of surface pores on drug-loaded fibers on eukaryotic and bacterial cell attachment was revealed. Porous electrospun CAM-loaded microfiber scaffolds (THF/DMSO) allow better fibroblast attachment and growth compared to the nonporous electrospun microfiber (THF/DMSO) and nanofiber scaffolds (AA/FA). Furthermore, the porous CAM-loaded microfiber scaffolds offer the best antibiofilm activity against *E. coli*. This study demonstrates the importance of designing the single fiber surface porosity in addition to the fiber diameter which may affect the drug release, mechanical properties,

https://dx.doi.org/10.1021/acsomega.0c04402
ACS Omega 2020, 5, 30011−30022

fiber−cell interactions, and antibiofilm activity of electrospun fiber scaffolds for wound infection treatment.

4. EXPERIMENTAL SECTION

4.1. Materials. *4.1.1. Polymer, Solvents, and Supplies.* PCL (M_n: 80,000) (15% w/v) was used as a carrier polymer for fiber formation. CAM (PubChem CID: 5959) was used as an antibacterial model drug. PCL, CAM, penicillin, streptomycin, and solvents—THF, DMSO, AA, FA, and formaldehyde—were obtained from Sigma-Aldrich, Inc. (Darmstadt, Germany). Growth media and buffers used in this study: Glasgow' minimal essential medium (GMEM) (PAN Biotech, GMBH Aidenbach, Germany), fetal bovine serum (FBS), tryptose phosphate broth (TPB, Difco, USA), 4-(2-hydroxyethyl)-1-piperazineethanesulfonic acid) (HEPES), Dulbecco's modified Eagle's medium (DMEM, phenol red, and serum-free medium) (Sigma-Aldrich Inc., Darmstadt, Germany), Lennox lysogeny broth (LB) (Sigma-Aldrich, Inc., Darmstadt, Germany), and all other materials were of reagent grade and were used as received without any further purification.

4.2. Electrospinning of Fiber Scaffolds. Solutions were allowed to mix overnight with the aid of a magnetic stirrer. Drug (CAM) was added to the electrospinning solution after polymer (PCL) dissolution in solvent mixtures and was further stirred for 1 h before electrospinning. The amount of CAM was 4% w/w based on the dry weight of the solid material. Electrospinning of fiber scaffolds with and without CAM was performed, as previously described.[20] RH within an electrospinning chamber was varied depending on the fiber scaffold that was produced (porous *vs* nonporous) using a humidifier AEG LBF 7138 (EHT Haustechnik GmbH, Nürnberg, Germany). For the electrospinning of nonporous nanofibers and microfibers, the RH of 19% (low RH) was used, and for that of porous microfibers, 65% RH (high RH) was used. The applied voltage was varied between 11 and 15 kV. Electrospun fiber scaffolds were stored in airtight plastic zip-lock bags under ambient conditions (temperature of 22 ± 1 °C and RH of 20 ± 2%) until further analyses. Prior analyses, the samples were stored at 24 h under 0% RH in a desiccator.

4.3. Morphology and Structure of Electrospun Fibers. *4.3.1. Scanning Electron Microscopy.* The morphology, diameter, and surface topography of pristine PCL and CAM-loaded fibers were investigated using a scanning electron microscope (Zeiss EVO 15 MA, Germany). Randomly selected areas of fiber scaffolds were mounted on aluminum stubs and magnetron-sputter-coated with a 3 nm platinum layer in an argon atmosphere prior to microscopy. The mean fiber diameter was calculated (N = 100) and presented together with standard deviation (SD). The porosity and mean pore diameter of the fiber scaffolds have been reported previously.[20] In addition, the fiber scaffolds covered with eukaryotic cells were also visualized under a scanning electron microscope. For SEM analysis, the scaffolds were rinsed twice with 1× phosphate-buffered saline (1× PBS), pH 7.4, and then fixed with 4% formaldehyde for 30 min at RT. Then, they were rinsed twice with 1× PBS and dehydrated with increasing concentrations of ethanol (30, 60, and 96%). When dry, the SEM samples were prepared as described above.

4.3.2. Confocal Fluorescence Microscopy. CFM with a LSM710 (Carl Zeiss, Munich, Germany) and Zen software (Zeiss) were used for the visualization of fibroblast cells after the cell attachment and growth studies. After 48 h of cell attachment experiment, scaffolds were removed from the inserts and washed in 1× PBS solution, after which they were placed in 5 μg/mL FM 4-64 (Invitrogen, Thermo Fischer, USA) staining solution in DMSO. After 2 min, the scaffolds were removed and placed on a microscope slide and visualized under the microscope. To evaluate the cell penetration through the fiber scaffolds or view them, 3D micrographs were constructed using the z-stack images from CFM using Zen software. The z-stack image consisted of 101 slices with a depth of 134.95 μm, and the cell infiltration was measured using 3D measurements.

4.4. Mechanical Analysis. Mechanical behavior of the dry and wet fiber scaffolds was studied using a Brookfield CT3 Texture Analyzer (Middleboro, MA, USA) equipped with a 10 kg load cell. The tensile test method was used for analysis in line with the ASTM D-638 and ISO10350:1993 mechanical testing guidelines. TexturePro CT software (AMTEK Brookfield, Middleboro, MA, USA) was used for data collection and analysis. Roller Cam accessory grips (TA-RCA; width of 25 mm) were used to fix the sample. Samples were mounted between holders at a distance of 50 mm, and the target value for distance was 60 mm. Tensile testing was performed at a strain rate of 1 mm/s and a trigger load of 1 g. Tests were performed using bell-shaped electrospun fiber scaffolds (with a length of 50 mm, a middle part of 10 mm, and widths of 20 mm from both sides and 10 mm in the middle). All measurements were performed under ambient conditions (at a temperature of 22 ± 1 °C and a RH of 20 ± 2%). For wet electrospun fiber scaffolds, the scaffolds were immersed in the biorelevant buffer solution (1× PBS) for 3 min or 24 h and then analyzed for their mechanical properties. Each sample group comprised at least 3−5 specimens. The mean thickness of the fiber scaffolds varied from 0.09 up to 0.11 mm measured using a Precision-Micrometer 533.501 (Scala Messzeuge, Dettingen, Germany) with a resolution of 0.01 mm. Young's modulus (MPa, linear region) and tensile strength (zero slope) were calculated from each corresponding stress−strain curve. The same TexturePro CT software was used to obtain the elongation at break (%) values.

4.5. Contact Angle, Swelling, and Early *In Vitro* Degradation. In order to understand the hydrophilic/hydrophobic nature of the fiber scaffolds and their wettability behavior, the contact angle between the fiber scaffolds (m = 11.5 ± 0.01 mg; size 2 × 2 cm) and biorelevant 1× PBS (pH 7.4) was measured by the sessile drop method (OCA 15EC, DataPhysics Instruments GmbH, Filderstadt, Germany). A drop of 1× PBS buffer solution (5 μL) was applied onto the fiber scaffolds. The contact angle measurements were taken at time points 0 and 30 s after the liquid drop touched the surface of the fiber scaffold. This test was carried out at RT (22 °C ± 0.3). The contact angle was analyzed using SCA20 software (DataPhysics Instruments GmbH, Filderstadt, Germany). Each sample was measured at least in triplicate.

For swelling index and weight loss measurements (early *in vitro* degradation), a set of 4 cm^2 square-shaped samples (N = 3) were cut from the fiber scaffolds, weighed, and then immersed in 10 mL of 1× PBS solution at 37 °C for 24 h. After that, the samples were placed on plastic Falcon Cell stainer sieves (mesh size: 40 μm) (Fisher Scientific, Thermo Fischer, USA) placed on a 50 mL Falcon tube to remove free surface solution and weighed. The swelling index and weight loss were calculated as reported previously.[61]

4.6. Biological Evaluation of Differently Designed Electrospun Fiber Scaffolds. *4.6.1. Eukaryotic Cells and*

https://dx.doi.org/10.1021/acsomega.0c04402
ACS Omega 2020, 5, 30011−30022

Culturing Media. Baby hamster kidney cells (BHK-21) were used for cell studies. Fibroblasts were grown in GMEM (500 mL) supplemented with 7.5% FBS, 11 mL of 2% TPB, 10 mL of 1 M HEPES, 100 μg/mL penicillin, and 100 μg/mL streptomycin. Cells were maintained at 37 °C in a 5% CO_2 incubator.

4.6.2. Eukaryotic Cell Attachment and Growth. Fiber scaffolds were placed into 24-well plates using cell crown inserts (CellCrown, Scaffdex Oy, Finland), 500 μL of BHK-21 cell suspension (consisting approximately 10,000 cells) was seeded on the scaffolds and 700 μL of pure DMEM with phenol red and serum was added. The number of cells was determined using trypan blue exclusion (Invitrogen, Thermo Fischer, USA). After 24 h of incubation, 500 μL of medium was added. After 48 h, the scaffolds were removed from the inserts, placed carefully in 1× PBS, and transferred to 400 μL of DMEM (phenol red and serum-free medium). Another 100 μL of DMEM was added and 80 μL of MTS reagent (K300-500, Biovision, USA) was also added. The cells were incubated at 37 °C and 5% CO_2. After 45 min, the scaffolds were removed, the obtained colored media were pipetted onto a 96-well plate, and absorbances were measured using a plate reader (Invitrogen, Thermo Fischer, USA) at 490 nm. The graphs show the MTS activity of cells. From the same experiment, cell attachment and proliferation were visualized by SEM and CFM, as explained in the section Morphology and Structure of Electrospun Fibers. At minimum, three technical replicates were performed.

4.6.3. Bacterial Strains and Preparation of Stocks. Clinically relevant for wound infection facultative anaerobic and Gram-negative bacterial strains (*E. coli* DSM no. 1103 (clinical isolate); *P. aeruginosa* DSM no.: 1117 (*P. aeruginosa*), blood isolate) used in this study were obtained from the Leibniz Institute DSMZ-German Collection of Microorganisms and Cell Cultures. Preparation of DMSO stocks is described in a study by Preem et al.[3,4] and in the Supporting Information.

4.6.4. Bacterial Attachment, Growth, and Biofilm Formation. The biofilm formation protocol was established based on the work of Brackman et al.[62] and was already proved suitable in our previous study.[3] The schematics of the biofilm formation experiment can be seen in Figure 7. The detailed explanation of the biofilm formation experiment is given in the Supporting Information.

4.7. Statistical Analyses. The results are expressed as an arithmetic mean ± SD. Statistical analysis was performed by applying one-way ANOVA and post hoc pairwise *t*-tests with MS Excel 365 software ($p < 0.05$). In case of multiple comparisons, Holm's method was used for adjusting *p*-values. The image analysis was performed and mean diameters of the fibers ($N = 100$) calculated using ImageJ software 1.52e (National Institutes of Health, Bethesda, MD, USA) were calculated.

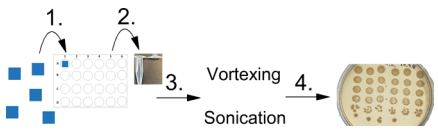

Figure 7. (1) One cm^2 square-shaped pieces of fiber scaffolds were placed in the medium (DMEM + FBS) with bacteria diluted to OD 0.05 (at 600 nm). (2) At each timepoint (24, 48, and 72 h), the sample was removed and placed in an Eppendorf tube with 1× PBS buffer. (3) The loose bacteria were rinsed twice with 1×PBS and put into 1 mL of fresh buffer in an Eppendorf tube after which the biofilm disruption process was conducted by vortexing and sonication. (4) After biofilm disruption, the sample was diluted and plated on LB agar plates.

■ ASSOCIATED CONTENT

Supporting Information

The Supporting Information is available free of charge at https://pubs.acs.org/doi/10.1021/acsomega.0c04402.

Bacterial stock preparation; bacterial attachment and biofilm study; SEM micrographs of surface pore analysis; SEM micrographs after the swelling experiment, confocal micrographs of cellular attachment and growth; SEM micrographs of fibroblasts; and bacterial growth and biofilm formation of *P. aeruginosa* (PDF)

■ AUTHOR INFORMATION

Corresponding Author

Karin Kogermann − *Institute of Pharmacy, University of Tartu, 50411 Tartu, Estonia;* orcid.org/0000-0002-6813-4828; Phone: +372 737 5281; Email: karin.kogermann@ut.ee; Fax: +372 737 5289

Authors

Georg-Marten Lanno − *Institute of Technology, University of Tartu, 50411 Tartu, Estonia*

Celia Ramos − *Institute of Pharmacy, University of Tartu, 50411 Tartu, Estonia*

Liis Preem − *Institute of Pharmacy, University of Tartu, 50411 Tartu, Estonia*

Marta Putriņš − *Institute of Technology, University of Tartu, 50411 Tartu, Estonia*

Ivo Laidmäe − *Institute of Pharmacy and Department of Immunology, Institute of Biomedicine and Translational Medicine, University of Tartu, 50411 Tartu, Estonia*

Tanel Tenson − *Institute of Technology, University of Tartu, 50411 Tartu, Estonia*

Complete contact information is available at: https://pubs.acs.org/10.1021/acsomega.0c04402

Author Contributions

The manuscript was written through contributions of all authors. All authors have given approval to the final version of the manuscript.

Notes

The authors declare no competing financial interest.

■ ACKNOWLEDGMENTS

This study is part of the national funding projects no PRG726 (K.K.) and PRG335 (M.P. and T.T.) (Estonian Ministry of Education and Research and Estonian Research Council). Additionally, this research was funded by the European Regional Development Fund through the Centre of Excellence for Molecular Cell Technology (2014-2020.4.01.15-0013) (M.P. and T.T.) and a Scholarship in Smart Specialisation Growth Areas (G.-M.L.). L'ORÉAL Baltic "For Women In Science" Fellowship 2018 (K.K.) with the support of the Estonian National Commission for UNESCO and the Estonian Academy of Sciences and the L'ORÉAL−UNESCO international program "For Women In Science" are acknowledged. Prof K. Kirsimäe, MSc and J. Aruväli are thanked for

SEM measurements. Dr. E. Zusinaite and Prof A. Merits are acknowledged for providing eukaryotic cell lab instructions and facilities.

REFERENCES

(1) Shalumon, K. T.; Anulekha, K. H.; Girish, C. M.; Prasanth, R.; Nair, S. V.; Jayakumar, R. Single Step Electrospinning of Chitosan/Poly(Caprolactone) Nanofibers Using Formic Acid/Acetone Solvent Mixture. *Carbohydr. Polym.* **2010**, *80*, 413−419.
(2) Qu, H.; Wei, S.; Guo, Z. Coaxial Electrospun Nanostructures and Their Applications. *J. Mater. Chem. A* **2013**, *1*, 11513−11528.
(3) Preem, L.; Mahmoudzadeh, M.; Putrinš, M.; Meos, A.; Laidmäe, I.; Romann, T.; Aruväli, J.; Härmas, R.; Koivuniemi, A.; Bunker, A.; Tenson, T.; Kogermann, K. Interactions between Chloramphenicol, Carrier Polymers, and Bacteria-Implications for Designing Electrospun Drug Delivery Systems Countering Wound Infection. *Mol. Pharm.* **2017**, *14*, 4417−4430.
(4) Zupančič, Š.; Preem, L.; Kristl, J.; Putrinš, M.; Tenson, T.; Kocbek, P.; Kogermann, K. Impact of PCL Nanofiber Mat Structural Properties on Hydrophilic Drug Release and Antibacterial Activity on Periodontal Pathogens. *Eur. J. Pharm. Sci.* **2018**, *122*, 347−358.
(5) Srikar, R.; Megaridis, C. M.; Yarin, A. L.; Bazilevsky, A. V. Desorption-Limited Mechanism of Release from Polymer Nanofibers. *Proc. ASME Int. Manuf. Sci. Eng. Conf.* **2008**, *2*, 465−474.
(6) Zupančič, Š.; Preem, L.; Kristl, J.; Putrinš, M.; Tenson, T.; Kocbek, P.; Kogermann, K. Impact of PCL Nanofiber Mat Structural Properties on Hydrophilic Drug Release and Antibacterial Activity on Periodontal Pathogens. *Eur. J. Pharm. Sci.* **2018**, *122*, 347−358.
(7) Preem, L.; Bock, F.; Hinnu, M.; Putrinš, M.; Sagor, K.; Tenson, T.; Meos, A.; Østergaard, J.; Kogermann, K. Monitoring of Antimicrobial Drug Chloramphenicol Release from Electrospun Nano-and Microfiber Mats Using UV Imaging and Bacterial Bioreporters. *Pharmaceutics* **2019**, *11*, 487.
(8) Adeli, H.; Khorasani, M. T.; Parvazinia, M. Wound Dressing Based on Electrospun PVA/Chitosan/Starch Nanofibrous Mats: Fabrication, Antibacterial and Cytocompatibility Evaluation and in Vitro Healing Assay. *Int. J. Biol. Macromol.* **2019**, *122*, 238−254.
(9) Unnithan, A. R.; Barakat, N. A. M.; Tirupathi Pichiah, P. B.; Gnanasekaran, G.; Nirmala, R.; Cha, Y.-S.; Jung, C.-H.; El-Newehy, M.; Kim, H. Y. Wound-Dressing Materials with Antibacterial Activity from Electrospun Polyurethane-Dextran Nanofiber Mats Containing Ciprofloxacin HCl. *Carbohydr. Polym.* **2012**, *90*, 1786−1793.
(10) Sheets, K.; Wang, J.; Meehan, S.; Sharma, P.; NG, C.; Khan, M.; Koons, B.; Behkam, B.; Nain, A. S. Cell-Fiber Interactions on Aligned and Suspended Nanofiber Scaffolds. *J. Biomater. Tissue Eng.* **2013**, *3*, 355−368.
(11) Zhang, Y.; Lim, C. T.; Ramakrishna, S.; Huang, Z.-M. Recent Development of Polymer Nanofibers for Biomedical and Biotechnological Applications. *J. Mater. Sci.: Mater. Med.* **2005**, *16*, 933−946.
(12) Jeong, L.; Park, W. Preparation and Characterization of Gelatin Nanofibers Containing Silver Nanoparticles. *Int. J. Mol. Sci.* **2014**, *15*, 6857−6879.
(13) Yang, L.; Fitié, C. F. C.; van der Werf, K. O.; Bennink, M. L.; Dijkstra, P. J.; Feijen, J. Mechanical Properties of Single Electrospun Collagen Type I Fibers. *Biomaterials* **2008**, *29*, 955−962.
(14) Sankar, S.; Sharma, C. S.; Rath, S. N.; Ramakrishna, S. Electrospun Fibers for Recruitment and Differentiation of Stem Cells in Regenerative Medicine. *Biotechnol. J.* **2017**, *12* (). DOI: DOI: 10.1002/biot.201700263.
(15) Chou, S.-F.; Woodrow, K. A. Relationships between Mechanical Properties and Drug Release from Electrospun Fibers of PCL and PLGA Blends. *J. Mech. Behav. Biomed. Mater.* **2017**, *65*, 724−733.
(16) Baker, B. M.; Gee, A. O.; Metter, R. B.; Nathan, A. S.; Marklein, R. A.; Burdick, J. A.; Mauck, R. L. The Potential to Improve Cell Infiltration in Composite Fiber-Aligned Electrospun Scaffolds by the Selective Removal of Sacrificial Fibers. *Biomaterials* **2008**, *29*, 2348−2358.
(17) Nam, J.; Huang, Y.; Agarwal, S.; Lannutti, J. Improved Cellular Infiltration in Electrospun Fiber via Engineered Porosity. *Tissue Eng.* **2007**, *13*, 2249.
(18) Han, Y.; Jiang, Y.; Li, Y.; Wang, M.; Fan, T.; Liu, M.; Ke, Q.; Xu, H.; Yi, Z. An Aligned Porous Electrospun Fibrous Scaffold with Embedded Asiatic Acid for Accelerating Diabetic Wound Healing. *J. Mater. Chem. B* **2019**, *7*, 6125−6138.
(19) Wang, T.; Feng, Z.-Q.; Leach, M. K.; Wu, J.; Jiang, Q. Nanoporous Fibers of Type-I Collagen Coated Poly(L-Lactic Acid) for Enhancing Primary Hepatocyte Growth and Function. *J. Mater. Chem. B* **2013**, *1*, 339−346.
(20) Ramos, C.; Lanno, G.-M.; Laidmäe, I.; Meos, A.; Härmas, R.; Kogermann, K. High Humidity Electrospinning of Porous Fibers for Tuning the Release of Drug Delivery Systems. *Int. J. Poymeric Mater. Polym. Biomater.* **2020**, 1.
(21) Tan, E. P. S.; Ng, S. Y.; Lim, C. T. Tensile Testing of a Single Ultrafine Polymeric Fiber. *Biomaterials* **2005**, *26*, 1453−1456.
(22) Chew, S. Y.; Hufnagel, T. C.; Lim, C. T.; Leong, K. W. Mechanical Properties of Single Electrospun Drug-Encapsulated Nanofibres. *Nanotechnology* **2006**, *17*, 3880−3891.
(23) Sebe, I.; Szabó, B.; Nagy, Z. K.; Szabó, D.; Zsidai, L.; Kocsis, B.; Zelkó, R. Polymer Structure and Antimicrobial Activity of Polyvinylpyrrolidone-Based Iodine Nanofibers Prepared with High-Speed Rotary Spinning Technique. *Int. J. Pharm.* **2013**, *458*, 99−103.
(24) Sebe, I.; Ostorházi, E.; Bodai, Z.; Eke, Z.; Szakács, J.; Kovács, N. K.; Zelkó, R. In Vitro and in Silico Characterization of Fibrous Scaffolds Comprising Alternate Colistin Sulfate-Loaded and Heat-Treated Polyvinyl Alcohol Nanofibrous Sheets. *Int. J. Pharm.* **2017**, *523*, 151−158.
(25) Zhang, H. J.; Kakizaki, T.; Uedono, A.; Taniguchi, Y.; Hayashi, K.; Hayashi, K. Effect of Free-Volume Holes on Dynamic Mechanical Properties of Epoxy Resins for Carbon-Fiber-Reinforced Polymers. *Macromolecules* **2017**, *50*, 3933−3942.
(26) Scheler, S.. The Polymer Free Volume as a Controlling Factor for Drug Release from Poly(Lactide-Co-Glycolide) Microspheres. *J. Appl. Polym. Sci.* **2014**, *131*. DOI: DOI: 10.1002/app.39740.
(27) D'Amato, A. R.; Bramson, M. T. K.; Corr, D. T.; Puhl, D. L.; Gilbert, R. J.; Johnson, J. Solvent Retention in Electrospun Fibers Affects Scaffold Mechanical Properties. *Electrospinning* **2018**, *2*, 15−28.
(28) Baji, A.; Mai, Y.-W.; Wong, S.-C.; Abtahi, M.; Chen, P. Electrospinning of Polymer Nanofibers: Effects on Oriented Morphology, Structures and Tensile Properties. *Compos. Sci. Technol.* **2010**, *70*, 703−718.
(29) Jiang, S.; Li, S. C.; Huang, C.; Chan, B. P.; Du, Y. Physical Properties of Implanted Porous Bioscaffolds Regulate Skin Repair: Focusing on Mechanical and Structural Features. *Adv. Healthcare Mater.* **2018**, *7*, 1700894−17.
(30) Kennedy, K. M.; Bhaw-luximon, A.; Jhurry, D. Cell-Matrix Mechanical Interaction in Electrospun Polymeric Scaffolds for Tissue Engineering : Implications for Scaffold Design and Performance. *Acta Biomater.* **2017**, *50*, 41−55.
(31) Shevchenko, R. V.; James, S. L.; James, S. E. A Review of Tissue-Engineered Skin Bioconstructs Available for Skin Reconstruction. *J. R. Soc., Interface* **2010**, *7*, 229−258.
(32) Pailler-Mattei, C.; Bec, S.; Zahouani, H. In Vivo Measurements of the Elastic Mechanical Properties of Human Skin by Indentation Tests. *Med. Eng. Phys.* **2008**, *30*, 599−606.
(33) Chen, S.; Liu, B.; Carlson, M. A.; Gombart, A. F.; Reilly, D. A.; Xie, J. Recent Advances in Electrospun Nanofibers for Wound Healing. *Nanomedicine* **2017**, *12*, 1335−1352.
(34) Pok, S. W.; Wallace, K. N.; Madihally, S. V. In Vitro Characterization of Polycaprolactone Matrices Generated in Aqueous Media. *Acta Biomater.* **2010**, *6*, 1061−1068.
(35) Croisier, F.; Duwez, A.-S.; Jérôme, C.; Léonard, A. F.; Van Der Werf, K. O.; Dijkstra, P. J.; Bennink, M. L. Mechanical Testing of Electrospun PCL Fibers. *Acta Biomater.* **2012**, *8*, 218−224.

https://dx.doi.org/10.1021/acsomega.0c04402
ACS Omega 2020, 5, 30011−30022

(36) Arinstein, A.; Zussman, E. Electrospun Polymer Nanofibers: Mechanical and Thermodynamic Perspectives. *J. Polym. Sci., Part B: Polym. Lett.* **2011**, *49*, 691−707.
(37) Gholipour Kanani, A.; Bahrami, S. H. Effect of Changing Solvents on Poly(ε-Caprolactone) Nanofibrous Webs Morphology. *J. Nanomater.* **2011**, *2011*, ID724153.
(38) Nelson, E. E.; Guyer, A. E. The Development of the Ventral Prefrontal Cortex and Social Flexibility. *Dev. Cogn. Neurosci.* **2011**, *1*, 233−245.
(39) Tammaro, L.; Saturnino, C.; D'Aniello, S.; Vigliotta, G.; Vittoria, V. Polymorphic Solidification of Linezolid Confined in Electrospun PCL Fibers for Controlled Release in Topical Applications. *Int. J. Pharm.* **2015**, *490*, 32−38.
(40) Cui, W.; Li, X.; Zhou, S.; Weng, J. Degradation Patterns and Surface Wettability of Electrospun Fibrous Mats. *Polym. Degrad. Stab.* **2008**, *93*, 731−738.
(41) Ma, M.; Mao, Y.; Gupta, M.; Gleason, K. K.; Rutledge, G. C. Superhydrophobic Fabrics Produced by Electrospinning and Chemical Vapor Deposition. *Macromolecules* **2005**, *38*, 9742−9748.
(42) Chau, T. T.; Bruckard, W. J.; Koh, P. T. L.; Nguyen, A. V. A Review of Factors That Affect Contact Angle and Implications for Flotation Practice. *Adv. Colloid Interface Sci.* **2009**, *150*, 106−115.
(43) Chou, S.-F.; Carson, D.; Woodrow, K. A. Current Strategies for Sustaining Drug Release from Electrospun Nanofibers. *J. Controlled Release* **2015**, *220*, 584−591.
(44) Yohe, S. T.; Colson, Y. L.; Grinstaff, M. W. Superhydrophobic Materials for Tunable Drug Release: Using Displacement of Air to Control Delivery Rates. *J. Am. Chem. Soc.* **2012**, *134*, 2016−2019.
(45) Farooque, T. M.; Camp, C. H.; Tison, C. K.; Kumar, G.; Parekh, S. H.; Simon, C. G. Measuring Stem Cell Dimensionality in Tissue Scaffolds. *Biomaterials* **2014**, *35*, 2558−2567.
(46) Sharifi, F.; Irani, S.; Zandi, M.; Soleimani, M.; Atyabi, S. M. Comparative of Fibroblast and Osteoblast Cells Adhesion on Surface Modified Nanofibrous Substrates Based on Polycaprolactone. *Prog. Biomater.* **2016**, *5*, 213−222.
(47) Wolf, K.; te Lindert, M.; Krause, M.; Alexander, S.; te Riet, J.; Willis, A. L.; Hoffman, R. M.; Figdor, C. G.; Weiss, S. J.; Friedl, P. Physical Limits of Cell Migration: Control by ECM Space and Nuclear Deformation and Tuning by Proteolysis and Traction Force. *J. Cell Biol.* **2013**, *201*, 1069−1084.
(48) Jalili-Firoozinezhad, S.; Mohamadzadeh Moghadam, M. H.; Ghanian, M. H.; Ashtiani, M. K.; Alimadadi, H.; Baharvand, H.; Martin, I.; Scherberich, A. Polycaprolactone-Templated Reduced-Graphene Oxide Liquid Crystal Nanofibers towards Biomedical Applications. *RSC Adv.* **2017**, *7*, 39628−39634.
(49) Mulhall, A.; de Louvois, J.; Hurley, R. Chloramphenicol Toxicity in Neonates: Its Incidence and Prevention. *Br. Med. J.* **1983**, *287*, 1424−1427.
(50) Loh, Q. L.; Choong, C. Three-Dimensional Scaffolds for Tissue Engineering Applications: Role of Porosity and Pore Size. *Tissue Eng., Part B* **2013**, *19*, 485−502.
(51) Abrigo, M.; Kingshott, P.; McArthur, S. L. Electrospun Polystyrene Fiber Diameter Influencing Bacterial Attachment, Proliferation, and Growth. *ACS Appl. Mater. Interfaces* **2015**, *7*, 7644−7652.
(52) De Cesare, F.; Di Mattia, E.; Zussman, E.; Macagnano, A. A Study on the Dependence of Bacteria Adhesion on the Polymer Nanofibre Diameter. *Environ. Sci.: Nano* **2019**, *6*, 778−797.
(53) Hu, M.-X.; Li, J.-N.; Guo, Q.; Zhu, Y.-Q.; Niu, H.-M. Probiotics Biofilm-Integrated Electrospun Nanofiber Membranes: A New Starter Culture for Fermented Milk Production. *J. Agric. Food Chem.* **2019**, *67*, 3198−3208.
(54) Cheng, Y.; Feng, G.; Moraru, C. I. Micro- and Nanotopography Sensitive Bacterial Attachment Mechanisms: A Review. *Front. Microbiol.* **2019**, *10*, 1−17.
(55) Hsu, L. C.; Fang, J.; Borca-Tasciuc, D. A.; Worobo, R. W.; Moraru, C. I. Effect of Micro- and Nanoscale Topography on the Adhesion of Bacterial Cells to Solid Surfaces. *Appl. Environ. Microbiol.* **2013**, *79*, 2703−2712.
(56) Anselme, K.; Davidson, P.; Popa, A. M.; Giazzon, M.; Liley, M.; Ploux, L. The Interaction of Cells and Bacteria with Surfaces Structured at the Nanometre Scale. *Acta Biomater.* **2010**, *6*, 3824−3846.
(57) Feng, G.; Cheng, Y.; Wang, S.-Y.; Hsu, L. C.; Feliz, Y.; Borca-Tasciuc, D. A.; Worobo, R. W.; Moraru, C. I. Alumina Surfaces with Nanoscale Topography Reduce Attachment and Biofilm Formation by Escherichia Coli and Listeria Spp. *Biofouling* **2014**, *30*, 1253−1268.
(58) Abrigo, M.; Kingshott, P.; McArthur, S. L. Bacterial Response to Different Surface Chemistries Fabricated by Plasma Polymerization on Electrospun Nanofibers. *Biointerphases* **2015**, *10*, 04A301.
(59) Li, X. Z.; Livermore, D. M.; Nikaido, H. Role of Efflux Pump(s) in Intrinsic Resistance of Pseudomonas Aeruginosa: Resistance to Tetracycline, Chloramphenicol, and Norfloxacin. Antimicrob. *Agents Chemother.* **1994**, *38*, 1732−1741.
(60) Morita, Y.; Tomida, J.; Kawamura, Y. Responses of Pseudomonas Aeruginosa to Antimicrobials. *Front. Microbiol.* **2013**, *4*, 1−8.
(61) Nazemi, K.; Moztarzadeh, F.; Jalali, N.; Asgari, S.; Mozafari, M. Synthesis and Characterization of Poly(Lactic-Co-Glycolic) Acid Nanoparticles-Loaded Chitosan/Bioactive Glass Scaffolds as a Localized Delivery System in the Bone Defects. *BioMed Res. Int.* **2014**, *2014*, ID898930.
(62) Brackman, G.; Cos, P.; Maes, L.; Nelis, H. J.; Coenye, T. Quorum Sensing Inhibitors Increase the Susceptibility of Bacterial Biofilms to Antibiotics in Vitro and in Vivo. *Antimicrob. Agents Chemother.* **2011**, *55*, 2655−2661.

https://dx.doi.org/10.1021/acsomega.0c04402
ACS Omega 2020, 5, 30011−30022